Spectroscopy of high spin states in ^{16}O and ^{20}Ne using the $(^{12}C,^{8}Be)(\alpha_0)$ reaction

S. J. Sanders,* L. M. Martz,† and P. D. Parker
A. W. Wright Nuclear Structure Laboratory, Yale University, New Haven, Connecticut 06520
(Received 14 May 1979)

Spins, parities, and α_0-decay branching ratios have been determined for a number of states in ^{16}O and ^{20}Ne using the $^{12}C(^{12}C,^{8}Be)^{16}O^*(\alpha_0)^{12}C$ and $^{16}O(^{12}C,^{8}Be)^{20}Ne^*(\alpha_0)^{16}O$ reactions. The ^{8}Be nuclei were detected at 0°, and the alpha particles from the decay of the excited states formed in the $(^{12}C,^{8}Be)$ reactions were detected over the range $40° \leq \theta_{lab} \leq 97°$, typically corresponding to a range in the heavy-recoil center-of-mass system of $50° \leq \theta_{RCM} \leq 120°$. Structure observed at an excitation energy of 22.5 ± 0.5 MeV in ^{16}O appears to correspond to an 8^+ state which is then a candidate for identification as the 8^+ member of the $K^\pi = 0^+$, 4p-4h rotational band. In ^{20}Ne we have confirmed a number of spin assignments for states below 16 MeV in excitation, and in addition we have made the following assignments: 16.63 MeV (7^-), 17.3 MeV (8^+), 21.08 MeV (9^-), and 22.87 MeV (9^-). All of the α_0 branching ratios for the strongly populated states in ^{20}Ne are found to be roughly 100%, with the exception of those for the 17.3 MeV (8^+) and 21.08 MeV (9^-) levels which are found to be 40% and 65%, respectively.

[NUCLEAR REACTIONS $^{12}C(^{12}C,^{8}Be)^{16}O^*(\alpha_0)^{12}C$, $^{16}O(^{12}C,^{8}Be)^{20}Ne^*(\alpha_0)^{16}O$, particle-particle angular correlations; $E_{lab} = 78$ MeV, $\theta_{^8Be} \approx 0°$. Deduce J^π, $\Gamma_{\alpha_0}/\Gamma_{total}$.]

I. INTRODUCTION

States which have large alpha-particle reduced widths and can be grouped into rotational bands are prominent features in the spectroscopy of light even-even nuclei. A simple alpha-cluster model can qualitatively explain[1,2] the selective population of these states through alpha-particle transfer reactions such as $(^6Li,d)$ and $(^7Li,t)$, the large alpha-particle decay widths of these states, and their identification as members of rotational bands, (e.g., the $K^\pi = 0^+$, 4p-4h band in ^{16}O.) As experimental studies of alpha-particle transfer reactions have been extended to higher excitation energies,[3,4] more examples of these selectively populated states have been found, but in most cases it has not been possible to extract much quantitative, spectroscopic information for these states from simple alpha-transfer data.[4] By determining such spectroscopic information for some of these more recently discovered states, it should be possible to relate them to the rotational bands of previously known cluster states at lower excitation energies. In the region of excitation energy most closely studied in the present experiment, a number of the previously studied rotational bands are expected to reach their SU(3) limits. The characteristics of the states comprising the rotational bands at the SU(3) limit—and beyond—are expected to be important in establishing the precise role of the alpha-cluster symmetries in these nuclei.

We made a preliminary attempt to extract spectroscopic information for these alpha-cluster states from angular correlations measured using the $(^7Li,t)(\alpha_0)$ reaction at $E(^7Li) = 48$ MeV with the tritons detected at $\theta_{LAB} = 10°$. The measured correlations were, however, substantially distorted from the simple $|P_J|^2$ patterns expected for $m = 0$, alpha-particle transfer; this distortion was evident in a shift of the quantization axis away from the recoil direction and in a damping of the first minima and the secondary maxima in these angular correlations. These effects reflect the $m \neq 0$ substate population which is allowed for the $(^7Li,t)$ reaction even with direct alpha-transfer at 0°, because of the $l = 1$, $\alpha + t$ configuration in ^7Li. DaSilveira[5] has shown that these distortions can be reproduced in a finite-range distorted-wave Born-approximation (DWBA) calculation, but such results are dependent on the assumption of a reaction mechanism and are therefore not suitable for extracting quantitative spectroscopic information. Therefore, in order to get around these problems, in the present experiment we have measured angular correlations utilizing the reactions $^{12}C(^{12}C,^{8}Be)^{16}O^*(\alpha_0)^{12}C$ and $^{16}O(^{12}C,^{8}Be)^{20}Ne^*(\alpha_0)^{16}O$ in order to determine the spins, parities, and alpha-decay widths for a number of alpha-cluster states at high excitation energies in ^{16}O and ^{20}Ne.

II. EXPERIMENTAL PROCEDURE

The measurements were carried out at the MP-1 tandem Van de Graaff accelerator facilities at Yale University. Beam intensities of approximately 150 nÅ of 78-MeV $^{12}C^{6+}$ were maintained on

target. The targets were self-supporting carbon foils (typically 100 $\mu g/cm^2$) and $^{10}B_2O_3$ (typically 70 $\mu g/cm^2$) evaporated onto thin (5 $\mu g/cm^2$) carbon foil backings onto which a thin (~3 $\mu g/cm^2$) gold film had been previously evaporated. For the correlation measurements the target normals were rotated 55° from the incident beam direction. The choice of $^{10}B_2O_3$ for the oxygen target was dictated by the need for a clear kinematic separation between the $^{16}O(^{12}C,^{8}Be)^{20}Ne^*(\alpha_0)^{16}O$ coincidences and the corresponding ^{8}Be-α coincidences from the other target components. A beam stop (3 mm in diameter) was located 6 cm from the target (see Fig. 1). The ^{8}Be's were detected near 0° in the laboratory system by detecting the two alpha particles from the decay of the $^{8}Be_{g.s.}$ ($E_{Binding} = -92$ keV) in fast coincidence ($\Delta t_r \approx 10$ nsec) using a single 450 mm^2, 1 mm thick Si(SB) detector in which the left and right halves were functionally isolated (similar to the detector described by Artz *et al.*[6]). The detector was mounted in the scattering chamber at 0° with respect to the incident beam; particles could enter the detector by passing on either side of the beam stop in an annulus $1.5° \lesssim \theta \lesssim 3.2°$. In order to prevent the forward-angle elastically scattered ^{12}C ions from reaching the detector, it was mounted inside a ≈12.5-cm long gas absorber filled to 20 p.s.i.a. with ^{14}N at −30°C. The entrance window of the cell was a 2 mg/cm^2 Havar foil; the areal density of the N_2 gas absorber was ≈20 mg/cm^2. The use of a gas absorber has the important advantage of minimizing the resolution deterioration resulting from nonuniformity of the absorber thickness, and the use of a low-Z absorber material has the additional advantage of minimizing straggling.

The detector was masked by a 5-mm wide strip covering the isolation gap which separated the two halves of the detector (oriented vertically) and by horizontal strips along the top and bottom of the detector to restrict its angular acceptance in the vertical direction. Using Monte Carlo techniques, the counting efficiency (see Fig. 2) and the effective angular acceptance for ^{8}Be detection were determined as a function of ^{8}Be energy and of the detector geometry. For the geometry shown in Fig. 1, it was calculated that the effective ^{8}Be solid angle ranged between 0.40 and 0.45 msr for the energies of interest. Because of the requirement that the ^{8}Be alpha particles be detected in fast coincidence with one in each half of the detector, the angular acceptance for ^{8}Be's was only $-1° \lesssim \theta_{lab} \lesssim 1°$, even though the detector covered the range of angles out to 3°, (see Fig. 2). The efficiency for counting $^{8}Be^*$ events in this geometry is very low (because of their much larger

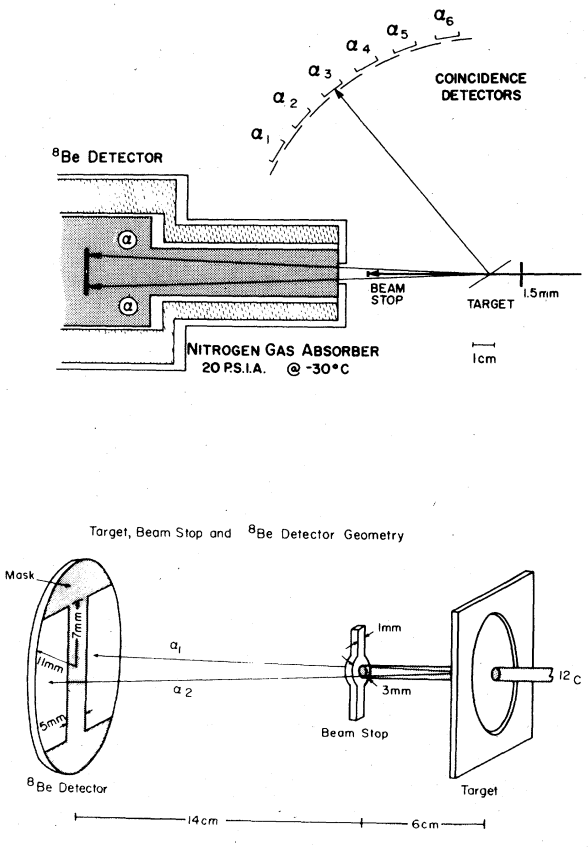

FIG. 1. Schematic diagram of the experimental apparatus showing the relative positions of the target, beam stop, ^{8}Be detector, and coincidence detectors.

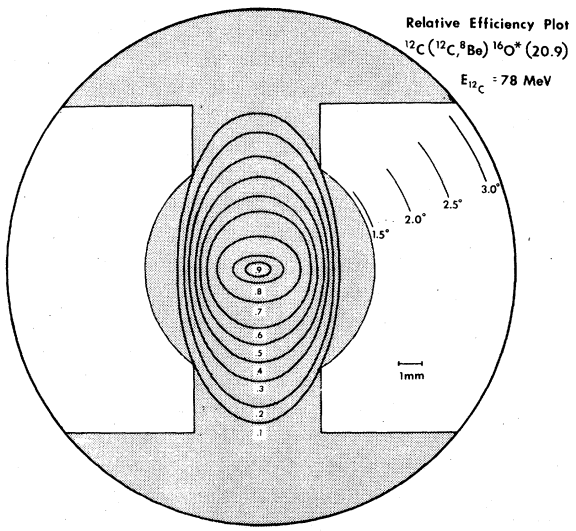

FIG. 2. Relative efficiency plot for detecting ^{8}Be events from the $^{12}C(^{12}C, ^{8}Be)^{16}O^*$ (20.9 MeV) reaction at an incident energy of 78 MeV. The detector geometry is assumed to be that of Fig. 1. Contours of equal efficiency are shown. The shading indicates regions of the detector which are masked.

breakup cone), and these events could be ignored.

Alpha particles from the decay of the excited states formed in the (^{12}C,^{8}Be) reactions were detected by an array of six 50-mm^2 surface barrier detectors mounted 12 cm from the target and spaced 10° apart (see Fig. 1), each with a solid angle of ≈2.7 msr in the laboratory. This detector array was moved in ≈3.3° steps to obtain data at 18 angles from approximately 40° to 99.7° in the laboratory.

The electronic instrumentation consisted of two fast and one slow coincidence networks. A singles event was defined by a fast coincidence between the two halves of the ^{8}Be detector ($\Delta t_r \approx 10$ nsec). A coincidence event required not only the ^{8}Be fast coincidence, but also a fast coincidence between one half of the ^{8}Be detector and one of the six coincidence detectors, as well as a subsequent slow coincidence ensuring that both fast coincidences had occurred within a suitable time window.

Data from these measurements were collected on-line using the laboratory IBM 360/44 computer-based data-acquisition-and-analysis system. For the present experiment the computer system was programmed to recognize eight different events: six coincidence events (corresponding to the six coincidence detectors), a singles event for the collection of a ^{8}Be spectrum for use in extracting alpha-particle decay widths, and a scalar event for monitoring the integrated beam current and the system dead time. For a singles event the computer was programmed to read in the outputs of four ADC's corresponding to the energies of each of the two ^{8}Be alpha particles, the summed energy of these two alpha particles, and the timing signal generated by the associated time-to-amplitude converter (TAC). For the coincidence events, in addition to the four quantities listed above, the energy of the alpha particle from the decay of the intermediate state in $^{16}O^*$ or $^{20}Ne^*$, and a TAC signal from the second fast coincidence were also read in. These data were analyzed on-line, and all events were also stored on magnetic tape for subsequent off-line reanalysis.

The data reduction is presented schematically in Fig. 3. Those events which satisfy the time and energy requirements on the ^{8}Be alpha particles were sorted into singles events and coincidence events on the basis of whether or not a second fast coincidence ($\Delta t_r \approx 10$ nsec) occurred between the ^{8}Be and a decay alpha particle in any of the six coincidence detectors. Coincidence events corresponding to alpha-particle decays of the intermediate nuclear state back to the ground state of the target nucleus were then extracted from a plot of E_α vs $E_{^8Be}$.

A typical example of the ^{8}Be identification spectrum (E_{α_1} vs E_{α_2}) is shown in Fig. 4. The central, diagonal band corresponds to ^{8}Be (g.s.) events; because of the very small breakup energy of the ground state of ^{8}Be, $E_{\alpha_1} \approx E_{\alpha_2}$ for all such events. Because the decay cone for the $^{8}Be^*(2^+)$ events is considerably larger than the angular acceptance of the detector, the only $^{8}Be^*(2^+)$ events that can be observed by the detector are those in which the two alpha particles emerge at nearly 0° and 180° in the $^{8}Be^*(2^+)$ center-of-mass system; consequently these alpha particles have very different energies in the laboratory and can be largely excluded by drawing a gate around the central band. (The wings on the side of the central band of the ^{8}Be identification spectrum result from the inelastic excitation of ^{12}C and its subsequent decay into an alpha particle and a ^{8}Be nucleus, with the alpha particle being detected in one side of the

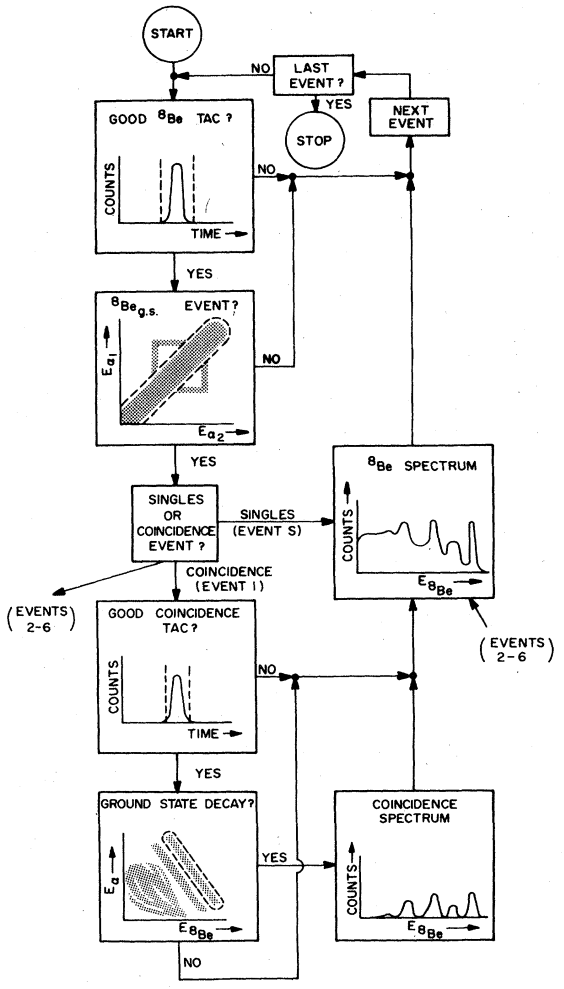

FIG. 3. Flow chart of the data reduction procedure. Events from six coincidence detectors are analyzed simultaneously.

0° detector and one of the ^{8}Be alpha particles being detected in coincidence in the other side of the split detector.)

Figure 5 shows a typical two-dimensional spectrum for the intermediate state alpha-particle decay (E_α vs E_{Be}), for the ^{12}C(^{12}C,^{8}Be)^{16}O*(α)^{12}C reaction. There is a clear separation between alpha particle decays to the ground state and to the first excited state of ^{12}C. Gates were drawn around the kinematic loci corresponding to each of these decays in order to extract coincidence data for the decay of the various intermediate states formed in the (^{12}C,^{8}Be) reaction. Similar data were obtained at each of the 18 coincidence angles.

III. EXPERIMENTAL RESULTS AND ANALYSIS

In comparison with an experiment measuring only singles events, the technique of measuring particle-particle angular correlations using the (^{12}C,^{8}Be)(α_0) reaction increases the experimental sensitivity for observing alpha-cluster states; in the coincidence experiment *both* the initial (^{12}C,^{8}Be) transfer reaction and the subsequent (α_0) decay are proportional to the alpha-particle width $\Gamma_{\alpha 0}$ of the intermediate state. The (^{12}C,^{8}Be) reaction is found to be just as selective in populating these states as the (^{7}Li,t) reaction, and the $J^\pi = 0^+$ character of all the participating nuclei (except for the intermediate nuclear state with spin J) coupled with the 0° detection of the ^{8}Be results in particularly simple $|P_J(\cos\theta)|^2$ angular distributions for the decay alpha-particles, provided that the intermediate levels are sufficiently isolated so that their angular correlations are characteristic of single states. [Since we are dealing with unbound states in the continuum, the striking selectivity of the (^{12}C,^{8}Be)(α_0) reaction is very important in helping to satisfy this requirement for isolated, single states.]

In Figs. 6 and 7, the ^{8}Be singles spectra for ^{16}O and ^{20}Ne are compared to the corresponding (^{7}Li,t) spectra; the same, few, strongly populated states are observed in the (^{7}Li,t) and (^{12}C,^{8}Be) reactions. In ^{16}O there are more than a hundred known levels with $E_x < 25$ MeV; fewer than a dozen of these are populated with any significant strength in the ^{12}C(^{7}Li,t) and ^{12}C(^{12}C,^{8}Be) reactions—mainly members of the $K^\pi = 0^+$ and 0^- alpha-cluster bands. The same selectivity characterizes the ^{20}Ne data where (of the more than 50 known levels with $E_x < 12$ MeV) only five members of the ground-state $K^\pi = 0^+$ band and the $K^\pi = 0_1^-$ band are appreciably populated. These figures also show the ^{8}Be coincidence spectra, obtained by requiring a subsequent alpha-particle decay to the ^{12}C or ^{16}O ground state. (The inset in the ^{12}C(^{12}C,^{8}Be)^{16}O*(α_0)^{12}C spectrum shows the coincidence data in the neighborhood of the 20.9- and 22.5-MeV levels, obtained by summing spectra at angles corresponding to minima in the 20.9-MeV angular correlation in order to emphasize the location and significance of the structure at $E_\alpha \approx 22.5$ MeV which otherwise tends to be obscured by the tail of the very much stronger 20.9-MeV peak.)

There is a large continuum background at high excitation in the singles spectra of Figs. 6 and 7. For lithium projectiles it is commonly assumed that most of this background results from the breakup of the lithium nucleus in the Coulomb field of the target nucleus.[7] A similar breakup mechanism is undoubtedly also responsible for part of the background in the (^{12}C,^{8}Be) spectra, but other sources may also be important in these

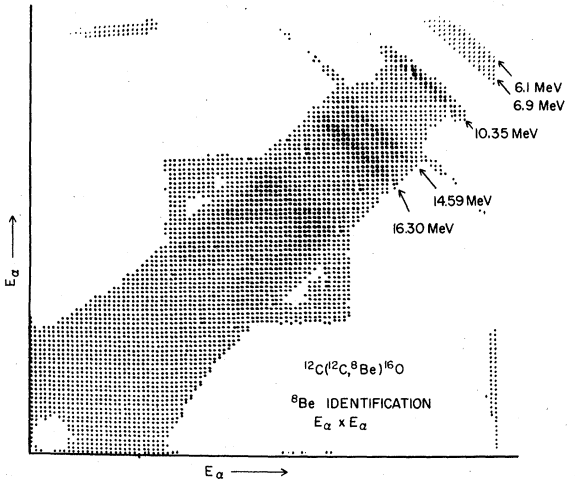

FIG. 4. Two-dimensional ^{8}Be identification plot. Labeled bands correspond to strongly excited states in ^{16}O. The origin of the wing structures flanking the central band is discussed in the text.

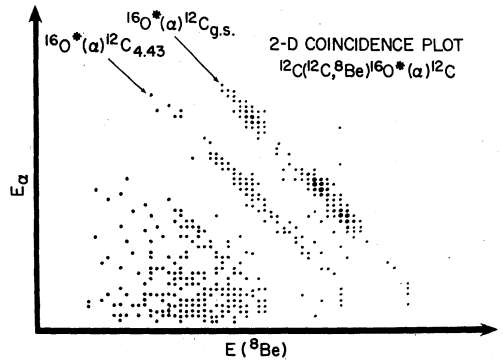

FIG. 5. Two-dimensional plot of the intermediate-state-decay alpha-particle energy vs the ^{8}Be energy. Clear separation is evident between alpha-particle decays to the ground state and first excited state of ^{12}C.

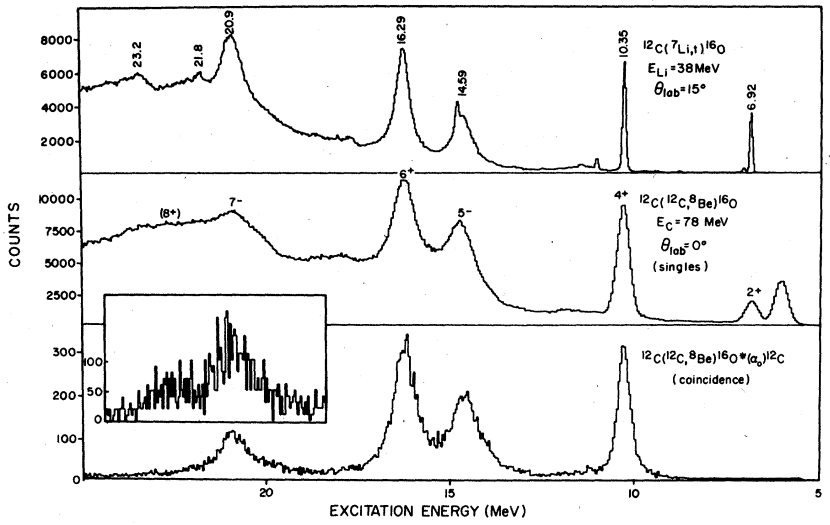

FIG. 6. Comparison of (^{7}Li,t), (^{12}C,^{8}Be), and (^{12}C,^{8}Be)(α_0) reactions leading to states of ^{16}O. The spin assignments are those observed in the present work. The inset emphasizes the structure near 22.5 MeV by showing the sum of the coincidence spectra at angles corresponding to minima in the 7$^-$ angular distribution.

cases. Whereas the $^{16}O(^7Li,t)^{20}Ne$ spectrum was measured using a gas target, the $^{16}O(^{12}C,^8Be)^{20}Ne$ spectrum was obtained using a $^{10}B_2O_3$ target evaporated onto a thin carbon foil, and reactions on the ^{12}C and ^{10}B in this target may also account for part of the background in this spectrum. The broad structure near $E_x \sim 19$ MeV in both of the (^{12}C,^{8}Be) singles spectra is caused by the inelastic excitation of the ^{12}C to a particle unbound state followed by its subsequent decay into $\alpha + {}^8Be$. (This structure corresponds to the "wing" structures on the side of the central, diagonal band in Fig. 4 as discussed above.) The requirement of an alpha decay back to the target ground state eliminates almost all of the background from the breakup of ^{12}C and from the excitation of a large number of continuum states with small alpha-particle widths. The coincidence spectra are suffi-

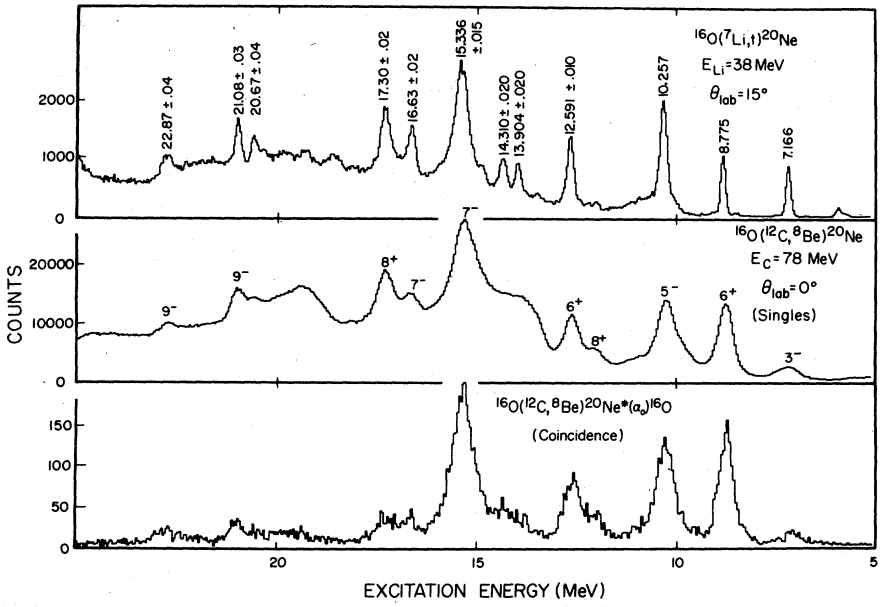

FIG. 7. Comparison of the (^{7}Li,t), (^{12}C,^{8}Be), and (^{12}C,^{8}Be)(α_0) reactions leading to states of ^{20}Ne. The spin assignments are those observed in the present work.

ciently clean to allow the angular correlations for most of these states to be extracted without background subtraction. Examples of these measured correlations are shown in Figs. 8 and 9 where we plot relative yields for the decay of $^{16}O^*$ or $^{20}Ne^*$ vs the decay angle in the recoil center-of-mass system (RCM).

Because the ^8Be's are detected at 0° and because all of the other nuclei which are involved in these reactions are spinless, the α_0 decay of any single, isolated state with spin J in the intermediate ^{16}O or ^{20}Ne nucleus has a simple $|P_J(\theta_{RCM})|^2$ angular dependence. The correlation asymmetries relative to 90° observed for the 4^+ and 6^+ states of ^{16}O probably result from coherent interferences among overlapping states. For these two states the magnitudes of the interference term were estimated to be less than 20% of the overall strength; this term was neglected in the subsequent analysis. Since all of the strongly populated states are measured at the same time, an internal calibration of the technique exists since the states whose properties are to be determined are measured and analyzed in parallel with states whose properties are already known.

The results of these analyses are summarized in Table I. In addition to the data shown in Figs. 8 and 9, correlations were also measured for the α_0 decay of ^{20}Ne excited states at 7.166, 8.775, 10.257, 11.95, and 15.336 MeV. The agreement between our results and previously determined assignments for several well-known states supports the credibility of our assignments for the

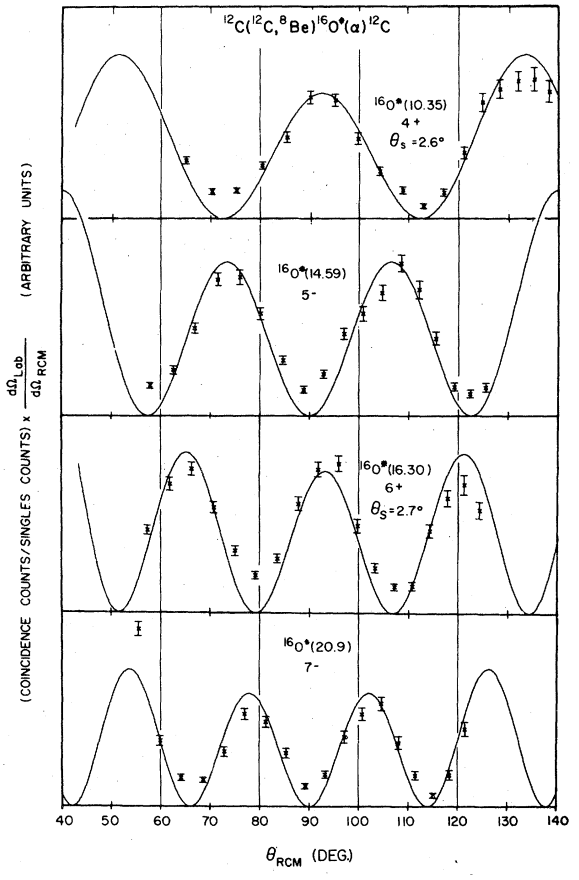

FIG. 8. Measured angular correlations for the $^{12}C(^{12}C,^8Be)^{16}O^*(\alpha_0)^{12}C$ reaction. The solid curves show $|P_J(\theta_{RCM}+\theta_s)|^2$ angular distributions, normalized to the data, where θ_s simulates shifts in the correlations caused by small admixtures of overlapping levels. For the 5⁻ and 7⁻ levels these shifts are negligible.

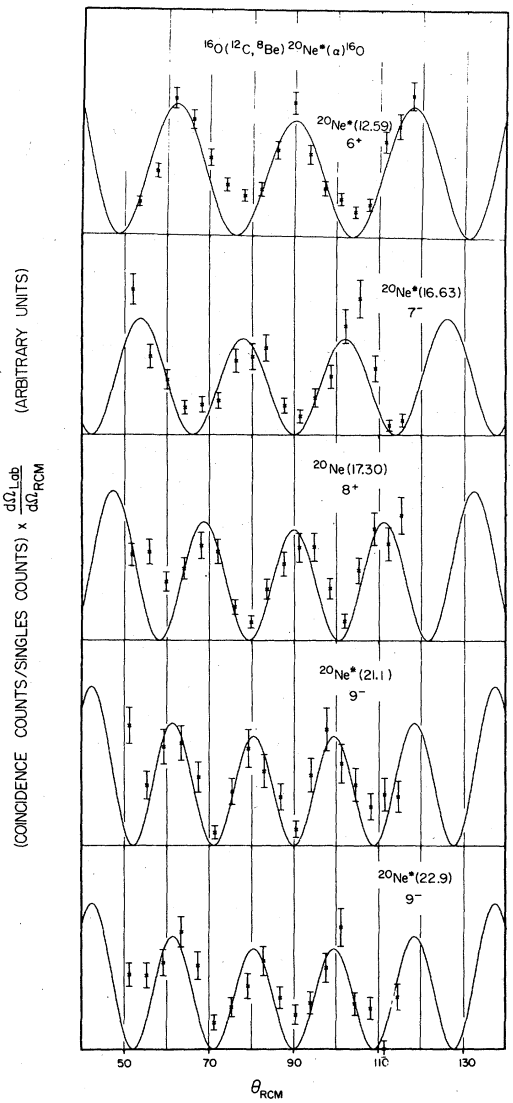

FIG. 9. Measured angular correlations for the $^{16}O(^{12}C,^8Be)^{20}Ne^*(\alpha_0)^{16}O$ reaction. The solid curves show $|P_J(\theta_{RCM})|^2$ angular distributions which are normalized to the data.

TABLE I. Summary of present experimental results. The excitation energies without quoted errors are from the Ajzenberg-Selove compilations (Ref. 8). The remaining excitation energies and the total widths for states in ^{20}Ne are from a reanalysis of (^7Li,t) data obtained by Cobern *et al.* (Ref. 4) (calibrated using known states below 12-MeV in excitation).

Nucleus	Excitation energy	J^π	Γ (keV)	$\frac{\Gamma_{\alpha_0}}{\Gamma}$	$\theta_{\alpha_0}^2$
^{16}O	10.35	4^+	--	0.90 ± 0.10	--
	14.59	5^-	--	0.75 ± 0.15	--
	16.3	6^+	--	0.90 ± 0.10	--
	20.9	7^-	--	--	--
	22.5 ± 0.5	(8^+)	--	--	--
^{20}Ne	7.166	3^-	--	--	--
	8.775	6^+	--	--	--
	10.257	5^-	145 ± 40	1	0.90 ± 0.25
	11.95	8^+	--	0.85 ± 0.15	--
	12.591 ± 0.010	6^+	110 ± 40	0.80 ± 0.10	0.26 ± 0.10
	15.336 ± 0.015	7^-	380 ± 60	0.90 ± 0.10	0.62 ± 0.12
	16.63 ± 0.02	7^-	190 ± 40	0.90 ± 0.10	0.17 ± 0.04
	17.30 ± 0.02	8^+	220 ± 40	$\geq 0.40 \pm 0.10$	$\geq 0.20 \pm 0.06$
	21.08 ± 0.03	9^-	100 ± 50	0.65 ± 0.15	0.10 ± 0.05
	22.87 ± 0.04	9^-	225 ± 40	0.90 ± 0.10	0.17 ± 0.04

other states.

The 22.5-MeV level in ^{16}O deserves some additional discussion, partly because the analysis of its data is not as unambiguous as the other cases and partly because our tentative assignment of $J^\pi = 8^+$ makes it a particularly interesting state. As noted above, the $^{12}C(^{12}C,^8Be)^{16}O^*(\alpha_0)^{12}C$ coincidence data (e.g., the inset in Fig. 6) clearly show the existence of a broad structure lying on the tail of the much more strongly populated 20.9-MeV (7^-) state. Assuming that this structure corresponds to a single state, angular correlations can be extracted in two ways.

At each angle the coincident yield between two fixed channel limits containing the 22.5-MeV state can simply be plotted as a function of θ_{RCM} after the usual lab to RCM coordinate system transformations. The resulting correlation clearly contains a very substantial contribution from the tail of the 20.9-MeV (7^-) state which must be included in any analysis of this correlation to extract spin-parity information for the 22.5-MeV state. This substantial 7^- admixture means that the correlation extracted in this way cannot be expected to have a simple $|P_J|^2$ pattern. In Fig. 10(a), we show the angular dependence of the correlation yield in the region around $E_x \approx 22.5$ MeV, with curves drawn through the data depicting the best fits assuming either a $7^- + 8^+$ or $6^+ + 7^-$ combination of states. The $7^- + 8^+$ combination is clearly preferred.

An alternate method for extracting this correlation takes the 20.9-MeV (7^-) state into account specifically, by subtracting from the coincidence yield the contribution due to the tail of the 20.9-MeV (7^-) state as determined by a Gaussian fit to its measured coincidence peak at the same laboratory

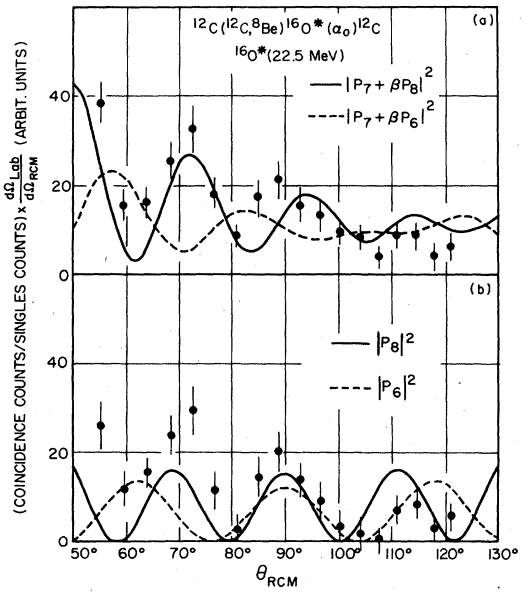

FIG. 10. Angular correlation yields in the region around $E_x \approx 22.5$ MeV in ^{16}O. In Part (a), the total correlation yield about 22.5 MeV is shown with curves drawn to indicate the best fits for distributions of the form $|P_J + \beta P_{J'}|^2$ where β is a complex number. For Part (b), background from the 20.9-MeV (7^-) state has been subtracted; in this case the curves shown have a pure $|P_J|^2$ angular dependence.

angle. (Lorentzian fits were also used but did not reproduce the measured data as well as the Gaussians; the Lorentzians tended to overemphasize the contributions of the tails. These differences were not major, however, and did not make any significant difference in the results of our analyses.) The net correlation resulting from this subtraction may well *still* contain admixtures from other states of various spins and parities, but the 22.5-MeV state should now be *more* dominant, and the pattern of the correlation should now be *more* characteristic of the spin-parity of this state. In Fig. 10(b), we show the correlation data in this region after the tail from the 20.9-MeV (7^-) state has been subtracted; simple $|P_6|^6$ and $|P_8|^2$ correlations are compared to these data. Although it is clear from the observed asymmetry in the correlation data extracted in this way that there are additional contributions from the admixture of states with the other J^π values, the periodicity is clearly that of an 8^+ state. Both of these methods have their own advantages. Both methods favor an assignment of $J^\pi = 8^+$ for this state which is then the first 8^+ level known in ^{16}O.

By comparing the integrated angular correlations with the yields in the singles spectra, these coincidence data can also be used to determine the branching ratio for α_0 decay which, when combined with the total width of the state, determines $\Gamma_{\alpha 0}$; the α_0 reduced width for the state $\theta_{\alpha 0}{}^2$ can then be evaluated as

$$\theta_{\alpha 0}{}^2 = \Gamma_{\alpha 0} \frac{2ma^2[F_l{}^2(k_{\alpha 0}a) + G_l{}^2(k_{\alpha 0}a)]}{6\hbar^2 k_{\alpha 0} a},$$

where

$$a = 1.25(A_{\text{core}}{}^{1/3} + 4^{1/3}) \text{ fm}.$$

These results are also summarized in Table I. The excitation energies and total widths supersede the results of Ref. 4. The related rotational bands in ^{16}O and ^{20}Ne are displayed in Figs. 11 and 12, combining the results in Table I with other relevant information from the compilations of Ajzenberg-Selove.[8]

As a qualitative check on these $\Gamma_{\alpha 0}/\Gamma$ branching ratios it is interesting to compare the coincidence spectra associated with decay to the ground state and

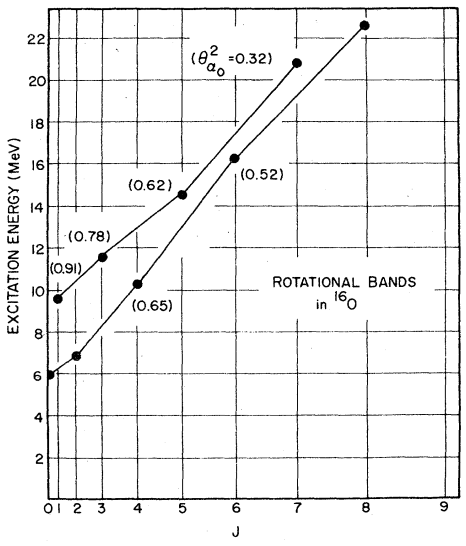

FIG. 11. The excitation energies for the $K^\pi = 0^+$ and 0^- rotational bands in ^{16}O plotted as functions of $J(J+1)$; the numbers in parentheses are the α_0 reduced widths for the states, as defined in the text.

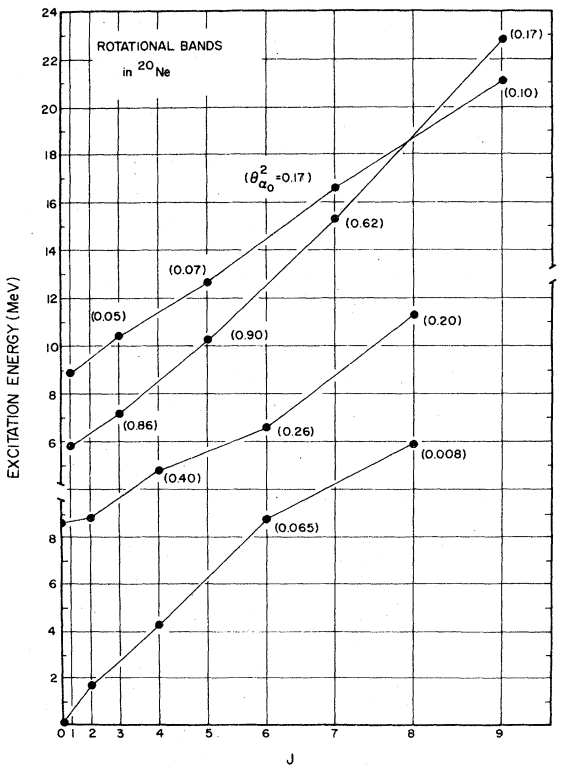

FIG. 12. Rotational bands in ^{20}Ne. The excitation energies of the members of these bands are plotted as functions of $J(J+1)$; the numbers in parentheses are the α_0 reduced widths for the states, as defined in the text. Note that the vertical scale has been split in order to separate visually the positive-parity bands from the negative-parity bands.

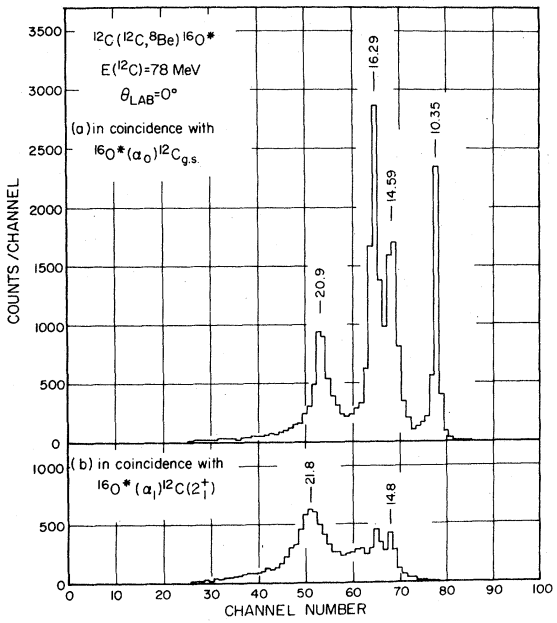

FIG. 13. Comparison of the correlation yield from states in ^{16}O decaying to the ground and first excited states in ^{12}C.

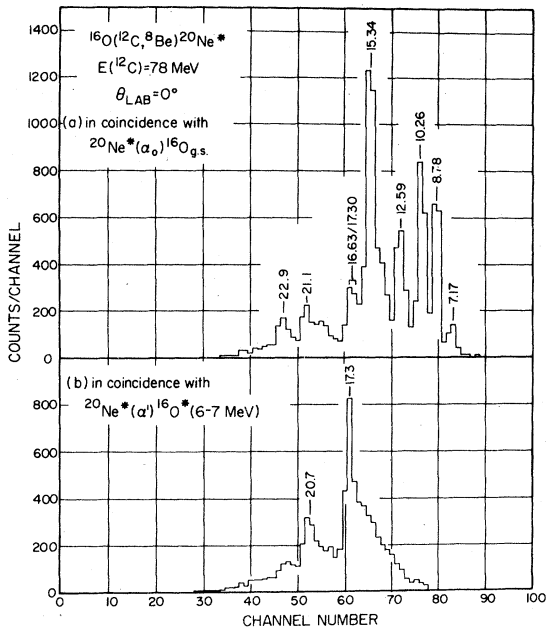

FIG. 14. Comparison of the correlation yield from states in ^{20}Ne decaying to the ground state of ^{16}O and to the low-lying excited states in ^{16}O, $E_x \approx 6$–7 MeV.

to the low-lying excited states. Figure 13 clearly shows the dominance of the $\alpha_0 + {}^{12}C_{g.s.}$ decay channel for the ^{16}O excited states at 10.35, 14.59, 16.29, and 20.9 MeV; the $\alpha_1 + {}^{12}C(2_1^+)$ decay of the broad 6^+ state at 21.8 MeV (Ref. 9) is also shown. In Fig. 14 the dominance of the $\alpha_0 + {}^{16}O_{g.s.}$ decay channel is clear for all the observed states except those at 17.3 and 21 MeV. The ^{8}Be-energy resolution in the present experiment is not adequate to separate the state at 17.30 MeV from the 9^- state reported[10] at $E_x = 17.40$ MeV with a >99% decay to ^{16}O* (6.13 MeV;3^-), so that it is not clear what fraction of the "17.3-MeV" peak in the ^{8}Be singles spectrum (Fig. 7) corresponds to each of these two states. It is clear that the $\alpha_0 + {}^{16}O_{g.s.}$ decays correspond to an 8^+ state at this energy with a substantial branch to this decay channel, but it is not clear whether the $\alpha + {}^{16}$O* decays correspond to this same 8^+ state or to the 9^- state at 17.40 MeV. In the (^{7}Li,t) data with better resolution (e.g., Fig. 7) it is the 17.30-MeV state that is populated rather than the 17.40-MeV state; on the basis of the very close resemblance between the (^{7}Li,t) and (^{12}C,^{8}Be) spectra in Fig. 7 for all the other states in ^{20}Ne, we would argue that the (^{12}C,^{8}Be) reaction is also populating primarily the 17.30-MeV state. [It can also be argued that the (^{12}C,^{8}Be) reaction is not likely to strongly populate the 17.40-MeV (9^-) state because of its very small (<1%) $\alpha_0 + {}^{16}O_{g.s.}$ width.] On the basis of these arguments we have interpreted the peak in the (^{12}C,^{8}Be) singles data and the $\alpha + {}^{16}$O coincidence data as corresponding to only the 17.30-MeV (8^+) state; our figure of 40% for the ground-state decay branch for this state is therefore a lower limit.

IV. DISCUSSION

The $K^\pi = 0^+$ and 0^- alpha-cluster bands in ^{16}O starting at 6.05 and 9.60 MeV, respectively, are shown in Fig. 11 on a standard excitation energy vs $J(J+1)$ rotational band plot. The broad $J^\pi = 8^+$ level tentatively identified at 22.5 MeV falls close to where the 8^+ member of the $K^\pi = 0^+$ band would be predicted based on a Regge trajectory extrapolation and has been included in this plot as a suggested member of the 0^+ band. This behavior is unlike that of the corresponding 8^+ member of the ground-state $K^\pi = 0^+$ rotational band in ^{20}Ne, where the observed level (at 11.95 MeV is several MeV below the energy predicted by such an extrapolation.

In the ^{20}Ne data, as shown in Fig. 12, the 6^+ state at 12.59 MeV and the 8^+ state at 17.30 MeV form

a natural extension of the excited $K^\pi = 0^+$ rotational band [8.6 MeV (0^+), 8.8 MeV (2^+) and 10.79 MeV (4^+)] which is suggested by Strottman *et al.*[11] to have primarily an (fp),[4] $(\lambda\mu) = (12\,0)$ configuration. The moment of inertia for this rotational band is much larger than that for the (8 0) ground-state band and is more similar to that for the $(fp)^4$ ground-state band in ^{44}Ti. In the resonating group method (RGM) calculations of Matsuse *et al.*[12] this band is found to involve substantial contributions from the (12 0) and higher (λ0) configurations. Because of the large spatial separation of the alpha cluster from the core in such configurations, they would be expected to have large alpha-particle reduced widths, in agreement with the results of our experiments and the results of the RGM calculations. [Earlier experiments[10,13] have given a 9^- assignment to a level at 17.4 MeV in ^{20}Ne. The state involved in the ^{12}C(^{12}C,α)^{20}Ne*(α)^{16}O correlations of Fifield *et al.*[10] has a ground-state decay branch of less than 1% and is therefore most probably not the same state studied in the present experiment which has a $\geq$40% ground-state decay branch. The ^{16}O(^{6}Li,d)^{20}Ne(α)^{16}O correlation experiment of Artemov *et al.*[13] is probably studying the same state as the present experiment (they also measure $\Gamma_{\alpha 0}/\Gamma = 0.4$), but because their correlations are limited to the range $130° \lesssim \theta_{RCM} \lesssim 175°$ they cannot distinguish as clearly between assignments of 8^+ or 9^-, as the present experiment.]

In ^{20}Ne there are two negative-parity $(sd)^3$ (fp) configurations which can be important in alpha transfer reactions, the well established $K^\pi = 0^-$ (90) band starting with the 5.79-MeV (1^-) state and a $K^\pi = 1^-$ (71) band[11] starting with the 8.86-MeV (1^-) state and probably containing an admixture of higher-order configurations. The two 7^- levels (15.34 and 16.63 MeV) and the two 9^- levels (21.08 and 22.87 MeV) seen in the present experiment fit very well into those two bands on the basis of their excitation energies and their α_0 reduced widths, as shown in Fig. 12. The two 9^- assignments are not confirmed by the Kurchatov group,[13] but they are in good agreement with the ^{16}O(α,α) elastic scattering results of Bergman and Hobbie.[14] The mixing of these two negative-parity bands can be analyzed in a manner similar to that suggested by Fortune *et al.*[15] to describe the mixing of positive-parity bands in ^{20}Ne. If it is assumed that the unperturbed $K^\pi = 1^-$ band has zero alpha-particle widths, then the interaction energy

$$H_{12} = \{|\theta_1/\theta_2|^2/[1 + (\theta_1/\theta_2)^2]\}(E_1 - E_2)$$

is found to be roughly constant (within the ~25% uncertainties in the reduced width measurements) for the $J^\pi = 1^-$, 3^-, 5^-, 7^-, and 9^- members of these bands and to be equal to about 600 keV which is comparable to values found by Fortune *et al.*[15] for the mixing between the $K^\pi = 0_2^+$ and 0_4^+ bands in ^{20}Ne.

In summary, we have shown that the (^{12}C,^{8}Be) reaction has the same high selectivity for alpha-cluster states as the (^{7}Li,t) reaction and that the measurement of (^{12}C,^{8}Be) (α_0) angular correlations provides an effective method for determining spins, parities, and branching ratios for alpha-cluster states in light nuclei. The new high-spin assignments made to high-lying states in ^{16}O and ^{20}Ne by the present experiment extend previously known rotational bands and are consistent with an alpha-cluster model for these nuclei.

This work was supported by the U. S. Department of Energy, Contract No. EY-76-C-02-3074.

*Present address: Physics Division, Argonne National Laboratory, Argonne, Ill. 60439.
†Present address: Bell Laboratories, Holmdel, New Jersey 07733.

[1]A. Arima, H. Horiuchi, K. Kubodera, and N. Takigawa, Adv. Nucl. Phys. 5, 345 (1972).
[2]H. Horiuchi, K. Ikeda, and Y. Suzuki, Progr. Theor. Phys. Suppl. 52, 89 (1972).
[3]K. Bethge, Annu. Rev. Nucl. Sci. 20, 255 (1970).
[4]M. E. Cobern, D. J. Pisano, and P. D. Parker, Phys. Rev. C 14, 491 (1976).
[5]E. F. DaSilveira, Contributions to the XIV Winter Meeting on Nuclear Physics—Bormio (1976); European Conference on Nuclear Physics with Heavy Ions-Caen (1976); Ph.D. thesis-Orsay (1977).
[6]J. L. Artz, M. B. Greenfield, and N. R. Fletcher, Phys. Rev. C 13, 156 (1976).
[7]R. W. Ollerhead, C. Chasman, and D. A. Bromley, Phys. Rev. 134, B74 (1964).
[8]F. Ajzenberg-Selove, Nucl. Phys. A190, 1 (1972); A281, 1 (1977): A300, 1 (1978).
[9]M. Avril, M. Lepareux, N. Saunier, A. Foti, G. Pappalardo, and A. Strazzeri, J. Phys. Lett. 36, 229 (1975).
[10]L. K. Fifield, R. W. Zurmühle, D. P. Balamuth, and J. W. Noé, Phys. Rev. C 8, 2203 (1973).
[11]D. Strottman, N. Anyas-Weiss, J. C. Cornell, P. S. Fisher, P. N. Hudson, A. Menchaca-Rocha, A. D. Panagioutou, and D. K. Scott, Phys. Lett. 47B, 16 (1973).
[12]T. Matsuse, M. Kamimura, and Y. Fukushima, Prog.

Theor. Phys. 53, 706 (1975).
[13]K. P. Artemov, V. Z. Gol'dberg, I. P. Petrov, V. P. Ruadkov, I. N. Serikov, and V. A. Timofeev, Yad. Fiz. 21, 1157 (1974) [Sov. J. Nucl. Phys. 21, 596 (1976)].
[14]C. Bergman and R. K. Hobbie, Phys. Rev. C 3, 1729 (1971).
[15]H. T. Fortune, R. Middleton, and R. R. Betts, Phys. Rev. Lett. 29, 738 (1972); Phys. Lett. 62B, 287 (1976).